Magnetoelasticity of $Fe_{1-x}Ga_x$ thin films on amorphous substrates

G. A. Ramírez [1,*] A. E. Moya Riffo,[2] J. E. Gómez,[3] D. Goijman [3] L. M. Rodríguez [3] D. Fregenal,[3] A. Butera [3] and J. Milano [3]

[1]*Comisión Nacional de Energía Atómica (CNEA); Consejo Nacional de Investigaciones Científicas y Técnicas (CONICET), Centro Atómico Bariloche, Av. Bustillo 9500, R8402AGP San Carlos de Bariloche, Argentina*

[2]*Comisión Nacional de Energía Atómica, Laboratorio Argentino de Haces de Neutrones, Centro Atómico Bariloche, R8402AGP San Carlos de Bariloche, Argentina*

[3]*Comisión Nacional de Energía Atómica (CNEA); Consejo Nacional de Investigaciones Científicas y Técnicas (CONICET), Centro Atómico Bariloche, Universidad Nacional de Cuyo (UNCUYO); Av. Bustillo 9500, R8402AGP San Carlos de Bariloche, Argentina*

In this work, we study the magnetoelastic behavior of $Fe_{1-x}Ga_x$ ($0.11 < x < 0.19$) thin films, grown on glass and oxidized Si(100) amorphous substrates, that present an isotropic crystalline texture in the film plane. The magnetoelastic coupling coefficients are obtained through the cantilever deflection technique. We find that the magnetoelastic response is larger for samples grown on glass with respect to those grown on Si(100), and such a response increases for larger Ga concentrations for both substrates used. Furthermore, the increasing substrate temperature during growth does not appear to have a significant effect on magnetoelastic behavior of samples grown on Si(100). From a model that takes into account the elastic grain interaction for isotropic systems, we are able to describe the experimentally observed behavior. We find that the magnetoelastic response of the samples grown on glass are well described by the Voigt model, while the samples on Si(100) present an intermediate response between the Voigt and Reuss models.

I. INTRODUCTION

Magnetostriction is defined as the change in the shape or the dimensions of a ferromagnetic material in response to an applied external magnetic field due to the magnetization reorientation. The phenomenon is quantified by the magnetostriction coefficient λ that describes the length variation in the direction of the applied field over the initial length. Magnetostrictive materials have been widely studied due to their potential application in sensors, actuators, energy harvesters, and spintronic devices [1–3]. In particular, $Fe_{1-x}Ga_x$ alloys (Fe-Ga) have attracted the attention of the scientific community for its high magnetostriction, large ductility and low costs with respect to alloys based on rare earths. The magnetostrictive properties of Fe-Ga have been shown to depend on the Ga concentration [4–6], and the maximum magnetostriction value ∼400 ppm is observed at $x \sim 0.19$. Although numerous theories have been proposed, the influence of the Ga and its contribution to the enhanced magnetostriction is still a subject under discussion [7–13].

For technological applications, it is necessary to grow the samples as thin films [14–16], which are rigidly bonded to the substrate and cannot deform freely when a magnetic field is applied. In this situation, the magnetostrictive effect produces a curvature in the film substrate system and for this reason it is appropriated to describe this behavior as a function of the magnetoelastic coupling (MEC) coefficients. As an example of this relation, the magnetoelastic energy for cubic systems can be expressed by two MEC coefficients B_1 and B_2, that are related to the magnetostriction constants [17]: $\lambda_{100} = -\frac{2}{3}\frac{B_1}{c_{11}-c_{12}}$ and $\lambda_{110} = -\frac{1}{3}\frac{B_2}{c_{44}}$, where c_{ij} are the material elastic constants.

Many authors have shown that MEC in thin films differs strongly from bulk materials [18–23]. This difference has been explained by means of models that describe this change in the MEC based on the competition between interface terms or higher-order deformation [17,21,24,25]. Previous works have reported measurements of MEC coefficients for Fe-Ga thin films grown on monocrystalline and amorphous substrates through indirect measurements that, due to the type of technique, present a large margin of error [26–28]. In Ref. [29], we have shown that the crystal grain structure can be controlled by the substrate type. For monocrystalline cubic substrates, the samples present a structural anisotropy in the plane due to substrate symmetry, which implies the existence of two independent MEC coefficients [12,13], while on amorphous substrates [or monocrystalline wafers with a native oxide, as on Si (100)], the samples present an isotropic behavior in the plane that can be described with a single MEC coefficient [19,24]. The single MEC coefficient for polycrystalline and isotropic films can be related to the B_1 and B_2 coefficients of a cubic structure, assuming a certain in-plane distribution for the orientation of individual crystallites [30]. A deeper knowledge of the behavior of the MEC coefficients of magnetostrictive thin films could be used to tailor samples with the desired magnetic properties.

In this contribution we report the MEC coefficients in sputtered Fe-Ga thin films determined by the cantilever deflection method [31]. We study sets of samples with different Ga

*gerardo.ramirez@cab.cnea.gov.ar

TABLE I. Detail of the sample sets studied. The error for the thickness is ± 5 nm and $\pm 0.5\%$ at for RBS composition.

Sample	Dep. params.		Thickness	RBS composition	
	T_s (°C)	$x_{\text{tgt}}^{\text{nom}}$	(nm)	$x_{\text{Fe}}^{\text{Film}}$	$x_{\text{Ga}}^{\text{Film}}$
FG17-G-RT	21	17	221	88.4	11.6
FG25-G-RT	21	25	218	83.9	16.1
FG30-G-RT	21	30	219	81.2	18.8
FG17-Si-RT	21	17	239	87.6	12.4
FG25-Si-RT	21	25	228	83.1	16.9
FG30-Si-RT	21	30	223	80.3	19.7
FG17-Si-250	250	17	217	87.7	12.3
FG25-Si-250	250	25	218	83.3	16.7
FG30-Si-250	250	30	219	80.6	19.4

concentrations, x, ranging from 0.11 to 0.19, grown onto glass and Si(100) substrates, setting the substrate temperature during growth at room temperature (RT) and 250 °C. The MEC coefficient behavior is studied by a magnetoelastic energy model based on the elastic average grain interaction approach.

II. EXPERIMENTAL

Fe-Ga thin films were grown by magnetron sputtering on glass and naturally oxidized Si(100) substrates from 3.8-cm diameter Fe-Ga alloy targets with nominal atomic compositions, $x_{\text{tgt}}^{\text{nom}} = 0.17$, 0.25, and 0.30. No thermal treatments were carried out on the Si(001) substrates prior to the sample deposition. The thickness of the oxide layer on such substrates was found to be ~ 2 nm, according to TEM studies previously reported [32]. The deposition process was carried out into a vacuum chamber where the substrate-target distance was fixed to ~ 5 cm using the following deposition conditions: Base pressure $<1.5 \times 10^{-6}$ Torr, argon pressure 2.7 mTorr, sputtering power 20 W, and deposition rates of $R_{0.17} \sim 0.136$ nm/s, $R_{0.25} \sim 0.144$ nm/s, and $R_{0.3} \sim 0.156$ nm/s, respectively. Three sets of three films each with the Ga concentrations, $x_{\text{tgt}}^{\text{nom}}$, were grown. The first set of samples was fabricated at RT on glass substrates, while the second one was also grown at RT but on Si substrates. The last set of samples was also fabricated on Si substrates using a substrate temperature (T_s) of 250 °C during the deposition. The samples were grown with nominal thicknesses of 200 nm on $\sim$100–150 μm thin substrates to facilitate flexing of the film/substrate system for magnetoelastic curvature measurements. The films studied in this work were labeled based on the type and temperature of the substrate, in addition to the nominal target Ga concentration, as summarized in Table I.

The chemical composition of the samples was determined by Rutherford backscattering (RBS) using a NEC 1.7 MeV Tandem accelerator with a NEC RC43 high vacuum end station attached, with 2 MeV He$^+$ ions [33]. The film thickness was also estimated by RBS measurements and confirmed by measuring the step height in a profilometer. Composition values measured in the samples were consistently lower than the nominal composition of the targets. This Ga loss during the growth process has been previously reported [29,34,35] and was attributed to the growth kinetics [29,36]. The composition ($x_{\text{Fe}}^{\text{Film}}$, $x_{\text{Ga}}^{\text{Film}}$) and thickness values of the samples are also summarized in Table I.

The structure and texture were characterized using a Panalytical Empyrean diffractometer equipped with a Cu X-ray tube (λ_{K_α}Cu = 0.15418 nm) and an Eulerian cradle. The crystal structure was determined using conventional Bragg-Brentano θ-2θ geometry, while the crystallographic texture was studied from pole figures using the so-called Schulz method [37].

The magnetometry study was performed by using a vibration sample magnetometer (VSM-Lakeshore 7404) with an applied field H along several in-plane angles ϕ_H.

We used the cantilever deflection method to measure the MEC coefficients. In this technique, a sample with a large length-to-width ratio ($\geqslant 3$) is mounted as a cantilever, i.e., it is fixed at one edge and the other is left free to allow the deflection of the cantilever [see Fig. 1(a)]. A laser beam is split into two beams that hit the sample at two positions (separated by millimeters), along its longest direction. The reflected beams reach two photodiodes (called fixed and free) that serve as position-sensitive detectors. The magnetostrictive effect is generated by applying an external magnetic field, $H_{\text{ext}} \sim 0.3$ T, large enough to saturate the magnetization of the sample along the H_{ext} direction. For this experiment we apply H_{ext} in two perpendicular directions H_x and H_y that induce a change in the curvature of the crystal as shown in Fig. 1(b). This causes a displacement of the reflected beams in the photodiodes, which results in a change in the measured voltage signal. To convert the voltage change into a position change of the reflected beams, it is necessary to calibrate the photodetectors. We carried out this calibration by moving the detectors horizontally by 10 μm using a micrometer screw. Thus, we correlated this known shift with the induced voltage change. Calibration factors were (0.61 ± 0.04) mV/m and (0.58 ± 0.04) mV/m for the fixed and the free detectors, respectively. Finally, the sample bending is quantified by the output signal changes of the detectors. Through these data and the consideration of the experimental geometry, the curvature change of the cantilever, $\Delta\kappa$, can be calculated considering the following expression [18,38,39]:

$$\Delta\kappa = \frac{\Delta_{\text{free}} - \Delta_{\text{fixed}}}{2l_{\text{spot}}l_{\text{PD}}}, \tag{1}$$

where Δ_{free} and Δ_{fixed} are the signal changes of the free and fixed detectors for two perpendicular magnetization directions, l_{spot} is the distance between the two laser spots at the sample surface, and l_{PD} is the distance between the sample and
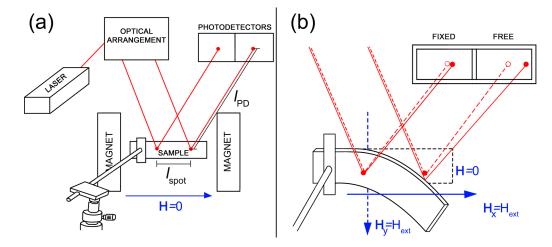
FIG. 1. (a) Experimental of the cantilever deflection method; l_{PD} is the distance between the sample and the photodetector and l_{spot} is the distance between the two laser spots at the cantilever sample. (b) Scheme of the cantilever sample in the unstressed state ($H = 0$) and the stressed state ($H = H_{ext}$) with the deflection of the beam. H_{ext} is applied in two perpendicular directions H_x, and H_y.

the photodetector. The curvature change $\Delta\kappa$ is proportional to the MEC coefficient B [13,23,40]:

$$B = \frac{Y_s d_s^2}{6(1 + \nu_s)d_F}\Delta\kappa, \qquad (2)$$

where Y_s is the substrate Young's modulus, d_s and d_F are the thicknesses of the substrate and film, respectively, and the ν_s is the substrate Poisson's ratio.

III. RESULTS

A. Structural

Figure 2 shows the diffractograms of sputtered Fe-Ga thin films deposited under different conditions. The XRD patterns were measured at $\chi = 30°$ from the sample normal in order to avoid overlapping peaks coming from the monocrystalline Si substrate. For all samples, three diffraction peaks can be distinguished at $2\theta \sim 44.2°$, $62.4°$, and $82.1°$ corresponding to the (110), (200), and (211) reflections of the A$_2$ Fe-Ga disordered phase. Also, we can observe a small diffraction peak at $2\theta \sim 54.8°$ in the samples grown on Si substrates with measured composition $x_{Ga}^{Film} \sim 0.19$ for all temperatures (FG30-Si-RT and FG30-Si-250 samples), which according to several authors is attributed to the (222) reflection of the DO$_3$ ordered phase. The metastable phase diagrams of bulk-Fe-Ga suggest that the samples showing this additional peak are in the zone of coexistence of phases A$_2$+DO$_3$, according to the range of composition and temperatures covered.

The diffractograms were refined by a simple full pattern Rietveld-type refinement model that has been developed to extract accurate lattice parameters, a, from a single XRD measurement of a textured multiphase sample [29]. We have found that a values increase slightly with the Ga concentration for A$_2$ Fe-Ga samples. This behavior has been extensively reported in the literature [41–44] and is attributed to the incorporation of Ga atoms into Fe lattice, due to the atomic radius of Ga (0.181 Å) being slightly greater than Fe (0.172 Å) [41].

The crystallographic texture of the samples was obtained for the (110), (200), and (211) reflections. From the experimental pole figures, the recalculated pole figures (RPF) and

the orientation distribution function (ODF) were determined using the MTEX code [45].

In previous works we showed how the ODF is calculated by using MTEX [29,34]. The RPF results for two representative samples: FG17-G-RT and FG17-Si-250 samples are shown in Figs. 3(a) and 3(b), respectively. We observed that all samples grown onto glass substrates do not present any preferential texture, that is, the crystallites in the films are randomly distributed.

This result is characterized by the little differences between maxima and minima of intensities in RPFs, as shown in Fig. 3(a) for FG17-G-RT. On the contrary, samples grown onto Si(100) substrates show two weak fiberlike textures, where the (113) and (111) are oriented normally to the film plane, as shown in Fig. 3(b) for FG17-Si-250. This analysis also indicates that samples with fiberlike texture present an in-plane isotropic behavior similar to the samples with a random distribution. The portion weight results suggest that the texture in both Si samples studied is similar.

B. Magnetic structure

Figure 4 shows the hysteresis loops for three representative samples (FG17-G-RT, FG17-Si-RT, and FG17-Si-250), in which **H** was applied at several in-plane substrate directions ϕ_H. The saturation magnetization decreases from 1500 to 1100 kA/m as x_{Ga}^{Film} increases. This behavior has been observed for all the studied samples and was attributed to a reduced average magnetic moment per Fe atom when the Fe content decreases [43,44] (see Table I). Also, we can observe that the type of substrate and the deposition temperature do not present a significant influence on the magnetization value [43].

The coercive field, $\mu_0 H_c$ (where μ_0 is the vacuum permeability, $\mu_0 = 4\pi \times 10^{-7}$ V s/A m), ranges from 1.43 to 5.14 mT and the normalized remanent magnetization M_r/M_s from 0.84 to 0.93. We observed that samples grown onto glass substrates present a small uniaxial anisotropy, probably related to spatial inhomogeneities during the sputtering process. This result is characterized by the small difference between
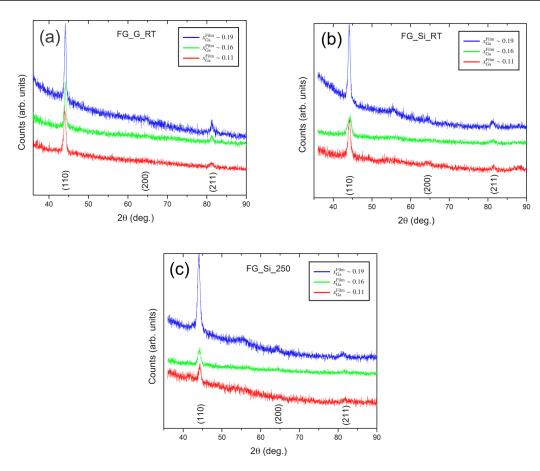
FIG. 2. XRD patterns for (a) Fe-Ga on glass, (b) Fe-Ga on Si RT, and (c) Fe-Ga on Si 250 °C. The red, green, and blue lines for each case correspond to samples at $x = 0.11$, 0.16 and 0.19, respectively. Diffractograms were measured at $\chi = 30°$ from the sample normal.

M_r/M_s and $\mu_0 H_c$ along several field directions as shown Fig. 4(a) for $FG17 - G - RT$. Samples grown onto Si(100) substrates evidence the presence of a uniaxial anisotropy as
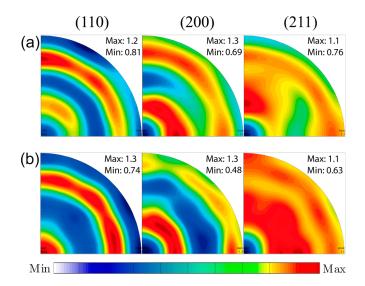

FIG. 3. Representation of RPFs for (a) FG17-G-RT and (b) FG17-Si-250 samples, obtained from the ODF. The color bar corresponds to the maximum and minimum intensity presented for each sample.

shown in Fig. 4(b) for FG17-Si-RT. For these samples, the easy axis is along the $[100]_{Si}$ direction, indicated by the fact that M_r/M_s and $\mu_0 H_c$ values are higher for this direction. The hard axis is along the $[010]_{Si}$ direction, and it is characterized by a lower remanent magnetization and a smaller coercive field. It is interesting to note that, although the native Si oxide is amorphous, the anisotropy Fe-Ga axis aligns along one of the $\langle 100 \rangle$ crystallographic Si axes; this behavior was already observed for us in previous studies [29,35]. Finally, we have observed that the samples become more isotropic when we increase the sample temperature during the growth process, which is reflected by the fact that M_r/M_s and $\mu_0 H_c$ do not present significant variations along the different in-plane directions, as shown in Fig. 4(c) for FG17-Si-250.

C. Magnetostriction

Figure 5 shows the experimental data obtained for the curvature change $\Delta\kappa$ through a cycle in which the magnetic field is applied 25 s along the length, then 25 s along the width, and finally, another 25 s along the length for the FG17-Si-250 sample. Similarly, cantilever deflection measurements were carried out for each of the studied sample sets and the obtained $\Delta\kappa$ values are summarized in Table II.

From $\Delta\kappa$ we are able to calculate the B value for all the studied samples by using Eq. (2). The d_F values were measured by RBS and those of d_s by using a micrometer.
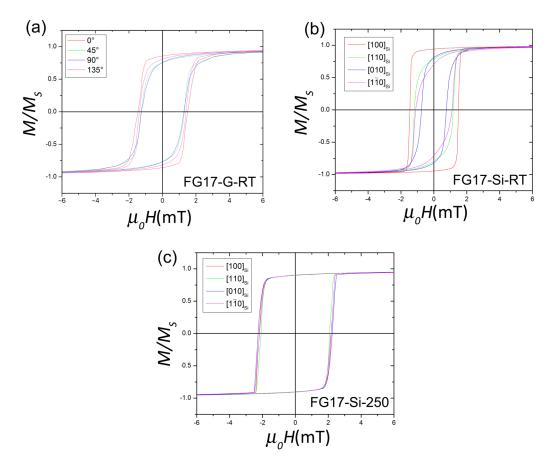
FIG. 4. M vs H loops for (a) Fe-Ga on glass, (b) Fe-Ga on Si RT, and (c) Fe-Ga on Si 250 °C, measured at different in-plane angles.

Y_s's were measured by the vibrating reed method [46,47] and the ν_s coefficients were extracted from Ref. [48]. All the parameters involved in the MEC coefficient calculations are shown in Table III and the values of B for the studied samples are presented in Table II.

Figure 6 shows the B values as a function of the $x_{\text{Ga}}^{\text{Film}}$ measured through the cantilever deflection method for the three sets of samples. The B values range from -3 to -9 MJ/m^3, depending on the Ga concentration, substrate type, and substrate temperature during growth. The fact that B's are negative indicates that the magnetoelastic energy is reduced when the films are subjected to a tensile stress, as we

have previously reported in Ref. [34], and this implies a positive magnetostriction. The B values found are in agreement with those reported by several authors [26–28].

Both sets of samples, on glass and Si, present the same main tendency; B has similar values for the two lower $x_{\text{Ga}}^{\text{Film}}$ (~ 0.12 and ~ 0.16) and decreases for $x_{\text{Ga}}^{\text{Film}} \sim 0.19$. The samples grown on glass show systematically lower B values than those grown on Si, indicating a larger magnetoelastic response for the samples on glass. In the next section we will discuss this behavior. On the other hand, the Fe-Ga/Si(100) samples present a similar behavior when grown at RT and 250 °C. Only for $x_{\text{Ga}} \sim 0.19$, the sample grown at 250 °C presents

TABLE II. Magnetic parameters of Fe-Ga samples. We also present the $\Delta\kappa$ values used to estimate B. In the table, the associated errors are M_s ($\pm$ 100), $\Delta\kappa$ ($\pm$ 0.2), and B ($\pm$ 0.5).

Sample	x T_c (°C)	x $x_{\text{tgt}}^{\text{nom}}$	M_s (kA/m)	$\Delta\kappa$ (1/km)	B (MJ/m^3)
FG17-G-RT	21	17	1500	−4.6	−5.9
FG25-G-RT	21	25	1300	−5.4	−7.0
FG30-G-RT	21	30	1200	−5.6	−9.3
FG17-Si-RT	21	17	1500	−2.8	−2.9
FG25-Si-RT	21	25	1300	−3.0	−3.2
FG30-Si-RT	21	30	1200	−4.9	−5.3
FG17-Si-250	250	17	1400	−3.4	−3.6
FG25-Si-250	250	25	1200	−3.2	−3.7
FG30-Si-250	250	30	1100	−6.3	−6.9

TABLE III. Film and substrate parameters used in Eq. (2) for studied samples. In the table, the associated errors are Y_s (± 0.5), d_s (± 10), and d_F (± 5).

Sample	Substrate parameters			
	Y_s (GPa)	ν_s	d_s (μm)	d_F (nm)
FG17-G-RT	76.4	0.22	164	221
FG25-G-RT	76.4	0.22	165	218
FG30-G-RT	76.4	0.22	186	219
FG17-Si-RT	130.0	0.28	121	238
FG25-Si-RT	130.0	0.28	120	228
FG30-Si-RT	130.0	0.28	119	222
FG17-Si-250	130.0	0.28	116	217
FG25-Si-250	130.0	0.28	122	218
FG30-Si-250	130.0	0.28	119	219

a lower B value with respect to the sample fabricated at RT. The overall result observed on Si samples is expected if we take into account that the crystalline texture is similar for the two sets of samples grown on Si, as we show in Sec. III A.

IV. DISCUSSION

In order to gain a deeper understanding of the magnetoelastic behavior, we analyze the role played by the elastic properties in the magnetoelasticity. In particular, it is important to consider the averaging mechanism of crystallites in polycrystals, since the effective stiffness and compliance tensors are related, for instance, to the residual stresses in the samples [34] and also to the magnetoelasticity [49,50]. In the general case of an in-plane isotropic film with a fiberlike structure along the growth direction (the samples grown on Si in this work), the magnetoelastic-free energy can be derived
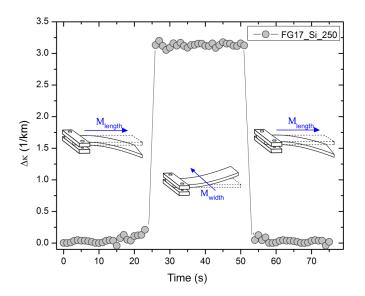

FIG. 5. Film curvature as a function of time of a typical cycle in which the magnetic field is applied 25 s in each direction for sample FG17-Si-250 measured at RT. M subscripts, width and length, indicate the magnetization direction.

from the expression for a tetragonal system [13]:

$$
\begin{aligned}
E_{\mathrm{me}}^{\mathrm{tet}} &= B_1^{\mathrm{tet}}\left(\varepsilon_{11}\alpha_1^2 + \varepsilon_{22}\alpha_2^2\right) + B_2^{\mathrm{tet}}\left(\varepsilon_{11}\alpha_2^2 + \varepsilon_{22}\alpha_1^2\right) \\
&\quad + B_3^{\mathrm{tet}}\varepsilon_{33}\alpha_3^2 + 4B_{3s}^{\mathrm{tet}}(\varepsilon_{13}\alpha_1\alpha_3 + \varepsilon_{23}\alpha_2\alpha_3) \\
&\quad + 4B_{1s}^{\mathrm{tet}}(\varepsilon_{12}\alpha_1\alpha_2),
\end{aligned}
\tag{3}
$$

where α_1, α_2, and α_3 are the direction cosines related to the magnetic moment orientation; ε_{ii} represents the strain along the i direction; and ε_{ij} is the shear strain associated to ij directions. B_1^{tet} and B_2^{tet} are the MEC coefficients related to the in-plane normal strains; B_3^{tet} is the normal strain in the perpendicular direction. Finally, B_{3s}^{tet} (B_{1s}^{tet}) represents the shear strain perpendicular (parallel) to the sample plane. By setting $B_{1s}^{\mathrm{tet}} = B_1^{\mathrm{tet}} = B_1^{\mathrm{fib}}$, we constrain the system to have a magnetoelastic isotropic behavior in the film plane as expected for a fiberlike system. For our study, $\alpha_3 = 0$, because the external magnetic field is applied in the film plane, then the terms related to α_3 can be discarded in Eq. (3). Moreover, to evaluate B, our experiment takes into account only the strain along the applied magnetic field direction (set along x or y axes at a time)[18]; this means that the surviving terms are those related purely with α_1 or α_2. Thus, Eq. (3) can be expressed for our fiberlike samples and measurement geometry as:

$$
E_{\mathrm{me}}^{\mathrm{fib}} = B_1^{\mathrm{fib}}\left(\varepsilon_{11}\alpha_1^2 + \varepsilon_{22}\alpha_2^2\right),
\tag{4}
$$

where B_1^{fib} corresponds to the MEC coefficient obtained experimentally via Eq. (2).

Now we proceed to derive a simple model for an isotropic system. This is the case of our samples on glass that will be correctly modeled because no texture was detected. However, we are also able to describe the Fe-Ga/Si samples with this simple isotropic model by taking into account that the microstructure of these samples presents a weak fiberlike texture as mentioned in Sec. III A.

For an isotropic system, it is possible to show that the magnetoelastic behavior can be modeled with an only MEC coefficient. Kittel in Ref. [51] derives this from the magnetoelastic energy of a cubic crystal, namely,

$$
\begin{aligned}
E_{\mathrm{me}}^{\mathrm{cub}} &= B_1^{\mathrm{cub}}\left(\varepsilon_{11}\alpha_1^2 + \varepsilon_{22}\alpha_2^2 + \varepsilon_{33}\alpha_3^2\right) \\
&\quad + 2B_2^{\mathrm{cub}}(\varepsilon_{12}\alpha_1\alpha_2 + \varepsilon_{23}\alpha_2\alpha_3 + \varepsilon_{31}\alpha_3\alpha_1).
\end{aligned}
\tag{5}
$$

By considering $B_1^{\mathrm{cub}} = B_2^{\mathrm{cub}} = B^{\mathrm{iso}}$, it is possible to show that $\lambda_{100} = \lambda_{111} = \lambda^{\mathrm{iso}}$. This fact assures that the same change in

length is obtained along any crystal direction [51], what is required in an isotropic system. Under these assumptions, λ^{iso} and B^{iso} are related in the following way:

$$\lambda^{\text{iso}} = -\frac{2}{3}\frac{B^{\text{iso}}}{c_{11}^{\text{iso}} - c_{12}^{\text{iso}}}, \tag{6}$$

where c_{11}^{iso}, c_{12}^{iso} are the elastic constants for the isotropic case that presents two independent elastic constants [52]. Taking into account that our isotropic polycrystal Fe-Ga samples are composed for cubic crystallites randomly arranged, we are able to use the following relation [53]:

$$\lambda^{\text{poly}} = \lambda^{\text{iso}} = \frac{2}{5}\lambda_{100} + \frac{3}{5}\lambda_{111}, \tag{7}$$

where λ_{100} and λ_{111} are the magnetostrictive constants for a single crystal that are directly related to the MEC and elastic constants through the following expressions [51]:

$$\lambda_{100} = -\frac{2}{3}\frac{B_1}{c_{11} - c_{12}}, \tag{8}$$

$$\lambda_{111} = -\frac{1}{3}\frac{B_2}{c_{44}}, \tag{9}$$

where c_{11}, c_{12}, and c_{44} are the independent elastic constants for a single crystal with cubic symmetry.

By replacing the expression for λ^{iso} given in Eq. (7) in Eq. (6), we arrive at the following expression for B^{iso}:

$$B^{\text{iso}} = \left(\frac{2}{5}\frac{B_1}{c_{11} - c_{12}} + \frac{3}{10}\frac{B_2}{c_{44}}\right)\left(c_{11}^{\text{iso}} - c_{12}^{\text{iso}}\right). \tag{10}$$

In that way we are able to express B^{iso} as a function of the MEC coefficients and the elastic constants of the cubic Fe-Ga single crystal and the ones corresponding to the polycrystal assumed as isotropic. Usually, the stiffness components in isotropic systems are expressed as a function of k and μ, which are related to c_{11}^{iso} and c_{12}^{iso} in the following way [52]:

$$c_{11}^{\text{iso}} = k + \frac{4}{3}\mu, \tag{11}$$

$$c_{12}^{\text{iso}} = k - \frac{2}{3}\mu. \tag{12}$$

Then, we can rewrite Eq. (10) as:

$$B^{\text{iso}} = \left(\frac{4}{5}\frac{B_1}{c_{11} - c_{12}} + \frac{3}{5}\frac{B_2}{c_{44}}\right)\mu. \tag{13}$$

The relation between μ and the elastic constants of the cubic single crystal depends on how the crystallites interact among them. In the literature, we can find different grain interaction models (with different degrees of complexity) that deal with the strain-stress states of the crystallite that compose the samples [54–57], and generally they have to be solved numerically. The simplest approaches are the Voigt [58] and Reuss [59] models. The Voigt-type averaging assumes that the crystallites are equally strained, while for Reuss the stresses are assumed to be constant along the sample [60–63]. These two models are the physical limits of the elastic behavior of crystals; however, the actual behavior is generally an intermediate state of those given for the Voigt- and Reuss-type
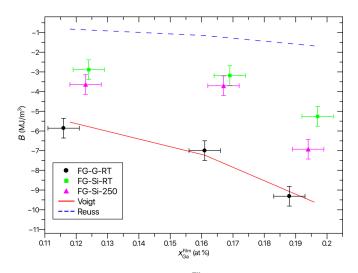

FIG. 6. B as a function of the $x_{\text{Ga}}^{\text{Film}}$ measured by the cantilever deflection method and limit values determined by the Reuss and Voigt models.

grain interaction. In the Voigt and Reuss limits, μ presents the following expressions [64]:

$$\mu_{\text{reuss}} = \frac{5G_1 \cdot G_2}{2G_2 + G_1}, \tag{14}$$

$$\mu_{\text{voigt}} = \frac{(2G_1 + 3G_2)}{5}. \tag{15}$$

where $G_1 = \frac{1}{2}(c_{11} - c_{12})$ and $G_2 = c_{44}$. Using these values for μ in Eq. (13), we calculate B^{iso} in the Voigt and Reuss limits. The calculated values are shown in Fig. 6. The elastic constants (c_{11}, c_{12} and c_{44}) and MEC coefficients (B_1 and B_2) corresponding to the Fe-Ga single crystal at different concentrations studied ($x_{\text{Ga}}^{\text{Film}} \sim 0.11$, 0.16, 0.19) were taken from Refs. [65] and [12], respectively. We can observe that the experimental B values for the samples grown on Si are within the range delimited by the Voigt and Reuss models. It is important to note that as the samples on Si show a weak fiber-like texture, then small deviations of the B values with respect to those calculated with our isotropic model can be found. For textured samples, more complex models were developed [54–56] in order to take into account the anisotropy due to the textures. On the other hand, for the samples grown on glass, B displays values compatible with a Voigt-type elastic behavior, indicating that the grain interaction occurs at constant strain for all crystallites. Although both substrates are amorphous, the results suggest that the film/substrate interaction plays an important role in the determination of the crystallographic and, therefore, in the magnetoelastic behavior. In order to understand the effect of such an interaction, we think that further studies on this topic should be focused on the joint treatment of the elastic properties of the films and substrates, with the goal to understand the mechanical behavior, particularly at the substrate/film interface.

V. CONCLUSIONS

In this work, the MEC coefficients of sputtered Fe$_{1-x}$Ga$_x$ thin films have been determined in order to study the

magnetoelastic response of samples grown on different substrates. Texture measurements reveal that all samples are isotropic in the film plane, allowing to describe the magnetoelasticity with a single MEC coefficient in such a plane.

The results show that the samples on glass present a larger magnetoelastic response with respect to those grown on Si(100). Focusing on the role played by the elastic properties, we propose a model based on the grain interaction model for isotropic systems, i.e., Voigt and Reuss limits. We have found that the samples grown on glass show a strong Voigt-type behavior while those on Si(100) show an intermediate behavior of the two models. Although both substrates are amorphous, the different values obtained for Si and glass suggest that the mechanical film/substrate interaction plays an important role in the magnetoelastic properties.

This work also shows that a deeper understanding of how the MEC coefficients depend on the crystallographic textures and also the film/substrate interaction could provide a new tool for manipulating the magnetoelastic properties in materials with potential use in straintronic devices.

[1] X. Zhao and D. Lord, Application of the Villari effect to electric power harvesting, J. Appl. Phys. **99**, 08M703 (2006).

[2] K. Ullakko, J. Huang, C. Kantner, and R. OHandley, Large magnetic field induced strains in Ni_2 MnGa single crystals, Appl. Phys. Lett. **69**, 1966 (1996).

[3] J. Atulasimha and A. Flatau, A review of magnetostrictive iron-gallium alloys, Smart Mater. Struct. **20**, 043001 (2011).

[4] A. Clark, J. Restorff, M. Wun-Fogle, T. Lograsso, and D. Schlagel, Magnetostrictive properties of body-centered cubic Fe-Ga and Fe-Ga-Al alloys, IEEE Trans. Magn. **36**, 3238 (2000).

[5] A. Clark, M. Wun-Fogle, J. Restorff, T. Lograsso, and J. Cullen, Effect of quenching on the magnetostriction on Fe_{1-x} Ga_x (0.13< x <0.21), IEEE Trans. Magn. **37**, 2678 (2001).

[6] P. B. Meisenheimer, R. A. Steinhardt, S. H. Sung, L. D. Williams, S. Zhuang, M. E. Nowakowski, S. Novakov, M. M. Torunbalci, B. Prasad, C. J. Zollner, Z. Wang, N. M. Dawley, J. Schubert, A. H. Hunter, S. Manipatruni, D. E. Nikonov, I. A. Y. L. Q. Chen, J. Bokor, S. A. Bhave, R. Ramesh, J.-M. Hu, E. Kioupakis, R. Hovden, D. G. Schlom, and J. T. Heron, Engineering new limits to magnetostriction through metastability in iron-gallium alloys, Nat. Commun. **12**, 2757 (2021).

[7] H. Cao, P. Gehring, C. Devreugd, J. Rodriguex-Rivera, J. Li, and D. Viehland, Role Of Nanoscale Precipitates On the Enhanced Magnetostriction of Heat-Treated Galfenol (Fe_{1-x} Ga_x) Alloys, Phys. Rev. Lett. **102**, 127201 (2009).

[8] M. Laver, C. Mudivarthi, J. Cullen, A. Flatau, W. Chen, S. Watson, and M. Wuttig, Magnetostriction and Magnetic Heterogeneities in Iron-Gallium, Phys. Rev. Lett. **105**, 027202 (2010).

[9] J. Boisse, H. Zapolsky, and A. Khachaturyan, Atomic-scale modeling of nanostructure formation in Fe-Ga alloys with giant magnetostriction: Cascade ordering and decomposition, Acta Mater. **59**, 2656 (2011).

[10] S. Guruswamy, T. Jayaraman, R. Corson, G. Garside, and S. Thuanboon, Short range ordering and magnetostriction in Fe-Ga and other fe alloy single crystals, J. Appl. Phys. **104**, 113919 (2008).

[11] H. Wang, Y. Zhang, R. Wu, L. Sun, D. Xu, and Z. Zhang, Understanding strong magnetostriction in Fe_{100-x} Ga_x alloys, Sci. Rep. **3**, 3521 (2013).

[12] A. Clark, K. Hathaway, M. Wun-Fogle, J. Restorff, T. Lograsso, V. Keppens, G. Petculescu, and R. Taylor, Extraordinary magnetoelasticity and lattice softening in bcc Fe-Ga alloys, J. Appl. Phys. **93**, 8621 (2003).

[13] M. Barturen, D. Sander, J. Milano, J. Premper, C. Helman, M. Eddrief, J. Kirschner, and M. Marangolo, Bulk-like behavior of magnetoelasticity in Fe_{1-x} Ga_x epitaxied thin films, Phys. Rev. B **99**, 134432 (2019).

[14] R. Basantkumar, B. Stadler, W. Robbins, and E. Summers, Integration of thin-film galfenol with MEMS cantilevers for magnetic actuation, IEEE Trans. Magn. **42**, 3102 (2006).

[15] H. Bhaskaran, M. Li, D. García-Sánchez, P. Zhao, I. Takeuchi, and H. Tang, Active microcantilevers based on piezoresistive ferromagnetic thin films, Appl. Phys. Lett. **98**, 013502 (2011).

[16] B. Adolphi, J. McCord, M. Bertram, C.-G. Oertel, U. Merkel, U. Marschner, R. Schafer, C. Wenzel, and W. Fischer, Improvement of sputtered galfenol thin films for sensor applications, Smart Mater. Struct. **19**, 055013 (2010).

[17] E. du Trémolet de Lacheisserie, Definition and measurement of the surface magnetoelastic coupling coefficients in thin films and multilayers, Phys. Rev. B **51**, 15925 (1995).

[18] D. Sander, The correlation between mechanical stress and magnetic anisotropy in ultrathin films, Rep. Prog. Phys. **62**, 809 (1999).

[19] O. Song, C. Ballentine, and R. O'Handley, Giant surface magnetostriction in polycrystalline Ni and NiFe films, Appl. Phys. Lett. **64**, 2593 (1994).

[20] G. Bochi, O. Song, and R. O'Handley, Surface magnetoelastic coupling coefficients of single-crystal fcc Co thin films, Phys. Rev. B **50**, 2043 (1994).

[21] R. Koch, M. Weber, K. Thurmer, and K.-H. Rieder, Magnetoelastic coupling of Fe at high stress investigated by means of epitaxial Fe(001) films, J. Magn. Magn. Mater. **159**, L11 (1996).

[22] A. Enders, D. Sander, and J. Kirschner, Strain dependence of the magnetic properties of nm Fe films on W(100), J. Appl. Phys. **85**, 5279 (1999).

[23] D. Sander, A. Enders, and J. Kirschner, Magnetoelastic coupling and epitaxial misfit stress in ultrathin Fe(100)-films on W(100), J. Magn. Magn. Mater. **198**, 519 (1999).

[24] G. Bochi, C. Ballentine, H. Inglefield, C. Thompson, and R. O'Handley, Evidence for strong surface magnetoelastic

anisotropy in epitaxial Cu/Ni/Cu(001) sandwiches, Phys. Rev. B **53**, R1729 (1996).

[25] K. Ha and R. C. O'Handley, Nonlinear magnetoelastic anisotropy in Cu/Ni/Cu/Si(001) films, J. Appl. Phys. **85**, 5282 (1999).

[26] D. Parkes, L. Shelford, P. Wadley, V. Holý, M. Wang, A. Hindmarch, G. van der Laan, R. Campion, K. Edmonds, S. Cavill, and A. Rushforth, Magnetostrictive thin films for microwave spintronics, Sci. Rep. **3**, 2220 (2013).

[27] N. Srisukhumbowornchai and S. Guruswamy, Large magnetostriction in directionally solidified FeGa and FeGaAl alloys, J. Appl. Phys. **90**, 5680 (2001).

[28] M. J. Jiménez, G. Cabeza, J. E. Gómez, D. Velázquez Rodríguez, L. Leiva, J. Milano, and A. Butera, Thickness dependence of the magnetoelectric coupling in Fe$_{89}$Ga$_{11}$ thin films deposited on ferroelectric PMN-PT single crystals, J. Magn. Magn. Mat. **501**, 166361 (2020).

[29] G. A. Ramírez, F. Malamud, J. E. Gómez, L. Rodríguez, D. Fregenal, A. Butera, and J. Milano, Controlling the crystalline and magnetic texture in sputtered Fe$_{0.89}$Ga$_{0.11}$ thin films: Influence of substrate and thermal treatment, J. Magn. Magn. Mat. **483**, 143 (2019).

[30] P. Bartolomé, A. Begué, A. Muñoz-Noval, M. Ciria, and R. Ranchal, Unveiling the different physical origin of magnetic anisotropy and magnetoelasticity in Ga-rich FeGa thin films, J. Phys. Chem. C **124**, 4717 (2020).

[31] J. Premper, D. Sander, and J. Kirschner, A combined surface stress and magneto-optical Kerr effect measurement setup for temperatures down to 30 K and in fields of up to 0.7 T, Rev. Sci. Instrum. **83**, 073904 (2012).

[32] C. Quinteros, M. Cortés Burgos, L. Albornoz, J. Gómez, P. Granell, F. Golmar, M. Luján Ibarra, S. Bustingorry, J. Curiale, and M. Granada, Impact of growth conditions on the domain nucleation and domain wall propagation in Pt/Co/Pt stacks, J. Phys. D **54**, 015002 (2021).

[33] S. Limandri, C. Olivares, L. Rodriguez, G. Bernardi, and S. Suárez, PIXE facility at centro atómico bariloche, Nucl. Instrum. Methods Phys. Res. B **318**, 47 (2014).

[34] G. A. Ramírez, A. Moya-Riffo, J. E. Gómez, F. Malamud, L. Rodríguez, D. Fregenal, G. Bernardi, A. Butera, and J. Milano, Influence of argon pressure on the structural properties of polycrystalline sputtered Fe$_{0.89}$Ga$_{0.11}$ thin films, Mater. Charact. **171**, 110790 (2021).

[35] G. A. Ramírez, A. Moya-Riffo, D. Goijman, J. E. Gómez, F. Malamud, L. Rodríguez, D. Fregenal, A. Butera, and J. Milano, Magnetocrystalline origin of the perpendicular magnetic anisotropy in Ga-poor FeGa thin films, J. Magn. Magn. Mater. **535**, 168047 (2021).

[36] L. Shaginyan, M. Misina, S. Kadlec, L. Jastrabik, A. Mackova, and V. Perina, Mechanism of the film composition formation during magnetron sputtering of WTi, J. Vac. Sci. Technol. A **19**, 2554 (2001).

[37] L. Schulz, A direct method of determining preferred orientation of a flat reflection sample using geiger counter X-ray spectrometer, J. Appl. Phys. **20**, 1030 (1949).

[38] K. Dahmen, S. Lehwald, and H. Ibach, Bending of crystalline plates under the influence of surface stress -a finite element analysis, Surf. Sci. **446**, 161 (2000).

[39] H. Ibach, The role of surface stress in reconstruction, epitaxial growth and stabilization of mesoscopic structures, Surf. Sci. Rep. **29**, 195 (1997).

[40] D. Sander and J. Kirschner, Cantilever stress measurements of ferromagnetic monolayers, Appl. Phys. A **87**, 419 (2007).

[41] A. Javed, N. Morley, and M. Gibbs, Structure, magnetic and magnetostrictive properties of as-deposited Fe-Ga thin films, J. Magn. Magn. Mater. **321**, 2877 (2009).

[42] A. Dunlap, N. Deschamps, R. Mar, and S. Farrell, Mossbauer effect studies of Fe$_{100-x}$ Ga$_x$ films prepared by combinatorial methods, J. Phys.: Condens. Matter **18**, 4907 (2006).

[43] J. M. Borrego, J. Blázquez, C. Conde, A. Conde, and S. Roth, Structural ordering and magnetic properties of arc-melted FeGa alloyss, Intermetallics **15**, 193 (2007).

[44] C. Bormio-Nunes, M. Tirelli, R. Sato, H. Müller, G. Wiesinger, H. Sassik, and M. Reissner, Volume magnetostriction and structure of copper mold-cast polycrystalline Fe-Ga alloys, J. Appl. Phys. **97**, 033901 (2005).

[45] R. Hielscher and H. Schaeben, A novel pole figure inversion method: Specification of the MTEX algorithm, J. Appl. Crystallogr. **41**, 1024 (2008).

[46] R. Schaller, G. Fantozzi, and G. Gremaud (Eds.), Preface of mechanical spectroscopy Q-1, *Mechanical Spectroscopy* (Trans Tech Publications Ltd., Switzerland, 2001).

[47] H. Colorado, H. Salva, C. Roldán, J. Vélez, and A. Ghilarducci, Internal friction and shear modulus of Ti$_{32}$ Zr$_{18}$ Ni$_{50}$ hydrogen storage alloy, Mater. Sci. Technol. **21**, 191 (2005).

[48] L. Zhang, R. Barrett, P. Cloetens, C. Detlefs, and M. Sánchez del Río, Anisotropic elasticity of silicon and its application to the modelling of X-ray optics, J. Synchrotron Radiat. **21**, 507 (2014).

[49] T. Duenas and G. Carman, Large magnetostrictive response of Terfenol-D resin composites (invited), J. Appl. Phys. **87**, 4696 (2000).

[50] P. Gergaud, C. Lallaizon, M. Putero, B. Lépine, O. Thomas, and A. Guivarc'h, Residual stresses and magnetoelastic coupling in ultrathin Fe films deposited on GaAs(001), MRS Proc. **615**, G2.9.1 (2000).

[51] C. Kittel, Physical theory of ferromagnetic domains, Rev. Mod. Phys. **21**, 541 (1949).

[52] V. Giurgiutiu, Fundamentals of aerospace composite materials, in *Structural Health Monitoring of Aerospace Composites* (Academic Press, Oxford, 2016), Chap. 2, pp. 25–65.

[53] E. W. Lee, Magnetostriction and magnetomechanical effects, Rep. Prog. Phys. **18**, 184 (1955).

[54] U. Welzel, M. Leoni, and E. Mittemeijer, The determination of stresses in thin films; modelling elastic grain interaction, Philos. Mag **83**, 603 (2003).

[55] U. Welzel, J. Ligot, P. Lamparter, A. Vermeulen, and E. Mittemeijer, Stress analysis of polycrystalline thin films and surface regions by X-ray diffraction, J. Appl. Crystallogr. **38**, 1 (2005).

[56] M. van Leeuwen., J.-D. Kamminga, and E. Mittemeijer, Diffraction stress analysis of thin films: Modeling and experimental evaluation of elastic constants and grain interaction, J. Appl. Phys. **86**, 1904 (1999).

[57] R. Vook and F. Witt, Thermally induced strains in evaporated films, J. Appl. Phys. **36**, 2169 (1965).

[58] W. Voigt, Ueber die beziehung zwischen den beiden elasticitatsconstanten isotroper korper, Ann. Phys. **274**, 573 (1888).

[59] A. Reuss, Berechnung der fliessgrenze von mischkristallen auf grund der plastizitatsbedingung fur einkristalle, Z. angew. Math. Mech. **9**, 49 (1929).

[60] E. Villalobos-Portillo, L. Fuentes-Montero, M. Montero-Cabrera, D. Burciaga-Valencia, and L. Fuentes-Cobas, Polycrystal piezoelectricity: revisiting the Voigt-Reuss-Hill approximation, Mater. Res. Express. **6**, 115705 (2019).

[61] R. de Wit, Elastic constants and thermal expansion averages of a nontextured polycrystal, J. Mech. Mater. Struct. **3**, 195 (2008).

[62] C. Kube and M. de Jong, Elastic constants of polycrystals with generally anisotropic crystals, J. Appl. Phys. **120**, 165105 (2016).

[63] J. den Toonder, J. van Dommelen, and F. Baaijens, The relation between single crystal elasticity and the effective elastic behaviour of polycrystalline materials: theory, measurement and computation, Model. Simul. Mater. Sci. Eng. **7**, 909 (1999).

[64] Z. Hashin and S. Shtrikman, A variational approach to the theory of the elastic behaviour of polycrystals, J. Mech. Phys. Solids **10**, 343 (1962).

[65] M. Wuttig, L. Dai, and J. R. Cullen, Elasticity and magnetoelasticity of Fe-Ga solid solutions, Appl. Phys. Lett. **80**, 1135 (2002).